Nonlinear mobility of the generalized Frenkel-Kontorova model

Oleg M. Braun,* Thierry Dauxois,† Maxim V. Paliy,* and Michel Peyrard
Laboratoire de Physique, URA-CNRS 1325, Ecole Normale Supérieure de Lyon, 46 Allée d'Italie, 69364 Lyon Cédex 07, France
(Received 5 June 1996)

Nonlinear mobility of one-and two-dimensional systems of interacting atoms in response to the dc external force is studied in the framework of a generalized Frenkel-Kontorova model. The atoms are subjected to a three-dimensional external potential periodic in two dimensions and parabolic in the third dimension. When the force increases, the system exhibits a transition from the low-mobility regime to the high-mobility regime, the latter corresponds to the running state of atoms in the inclined substrate potential. During the transition the system passes through intermediate states depending on whether the concentration of atoms corresponds to the ground-state atomic structure with the simple or complex elementary cell. All the transitions are first-order dynamical-phase transitions, i.e., they are discontinuous and exhibit a hysteresis even at nonzero system temperature. The simulation results are explained with the phenomenological approach, which treats a system of strongly interacting atoms as a system of weakly interacting quasiparticles (kinks).
[S1063-651X(97)02403-3]

PACS number(s): 46.10.+z, 05.70.Ln, 66.30.−h, 63.20.Ry

I. INTRODUCTION

The study of the atomic processes occurring at the interface of two materials when they are brought together, separated, and moved with respect to one another is central to many technological problems, such as adhesion, *contact formation, friction wear, lubrication, fracture*, etc. Owing to the development of new experimental and theoretical works for studying these phenomena at the atomic scale, an understanding is beginning to emerge of the molecular mechanisms of tribology in thin films and at surfaces; the atomic-force microscope from the experimental point of view or the molecular-dynamics simulations on massively parallel computers are, for example, very powerful tools for the physicist to acquire a better understanding of the underlying phenomena.

Here, we will consider one aspect of this problem: mass and charge transport in systems with strong interatomic interactions. We study particles, interacting with each other, adsorbed on a crystalline surface. The adsorbate is considered as a subsystem and the remainder is modeled as an external potential and a thermal bath. Such a system can be considered within the framework of the generalized Frenkel-Kontorova (FK) model. Introduced to model the dynamics of dislocations in crystals [1], the FK model describes in a more general context a system of interacting particles subjected to a periodic substrate (on-site) potential V_{sub}. This model may describe, for example, a closely packed row of atoms in crystals [2], a layer of atoms adsorbed on crystal surfaces [3], a chain of ions in a ''channel'' of quasi-one-dimensional conductors [4], hydrogen atoms in hydrogen-bonded systems [5], etc.

In the presence of thermal fluctuations, the particles may leave the original well and go to either the neighboring left or right well or they may move in the course of time to other wells which are further away: for long enough times the particles will diffuse in every direction. This activated diffusion mechanism of interacting particles was studied, for example, in a previous work [6]. If an additional force F is applied, the particle will preferably diffuse in the direction of this force and on the average there is a drift velocity that depends on the external force. For small forces, the mobility B defined by $\langle v\rangle = BF$ will be independent of the force (linear response), but for arbitrary forces F, the mobility will depend on it (nonlinear response). The problem is to calculate this nonlinear mobility.

Transport properties of the FK model have been a subject of intensive studies in the last decades. The linear mobility $B_0 = \langle v\rangle / F$, which describes the steady-state mean atomic velocity $\langle v\rangle$ in response to the dc driving force F in the limit $F \to 0$, was considered in a number of works (e.g., see [7] and references cited therein). In the general case, the mobility B should depend on F; the total external potential $V_{\mathrm{tot}}(x) = V_{\mathrm{sub}}(x) - Fx$ is a corrugated plane, with an average slope determined by the external force F. For large forces, $V_{\mathrm{tot}}(x)$ has no minima, whereas for intermediate and small forces, minima do exist. Denoting by ε the amplitude of the periodic potential, a its period, and C a numerical factor depending on the shape of the potential ($C=1$ for the sinusoidal potential), the barriers of the substrate potential become completely degraded for forces greater than $F_r \equiv C\pi\varepsilon/a$ and the system should behave as a homogeneous one; in this regime, the mobility $B(F)$ reaches its final value $B_f \equiv (m\eta)^{-1}$, where m is the atomic mass and η the viscous friction describing the energy exchange of the system under consideration with the thermostat.

The nonlinear mobility of the FK model has been studied only for the *overdamped* case (i.e., for the case $\eta \gg \omega_0$, where ω_0 is a characteristic frequency of atomic vibration in the external potential) with the trivial concentration $\theta = 1$ (the dimensionless atomic concentration θ is defined as the ratio of the number of atoms to the number of wells of the external potential). The low-temperature limit for the sine-Gordon

*Also at Institute of Physics, Ukrainian Academy of Sciences, 46 Science Avenue, UA-252022 Kiev, Ukraine.
†Electronic address: tdauxois@physique.ens-lyon.fr

(SG) case (i.e., for strong interatomic interaction) was investigated by Buttiker and Landauer [8] with the help of the generalized rate theory (see also [9]). In this case the magnitude of the atomic flux is restricted by the rate of creation of kink-antikink (kk) pairs [we recall that a kink (antikink) describes the minimally possible topologically stable local compression (extension) of the commensurate structure of the FK model]. The driving force lowers the barrier for the kk pair nucleation, and this results in the increase of system mobility. The rate theory is adequate only provided $F<F_r$ i.e., as far as the system dynamics have an activated nature. At high temperatures, the nonlinear mobility of the $\theta=1$ FK model was calculated within the random-phase (mean-field) approximation (RPA) [10,11]. In this case, the time-independent many-particle Schmoluchowsky equation may be reduced to a one-particle equation with an effective on-site potential and be solved numerically by the transfer-integral method. The calculations showed that for low external force as well as for high force the atomic flux is proportional to the force (Ohm's law), but the high-F mobility may be many orders of magnitude greater than the low-F mobility, so that the low-F and high-F regimes are separated by a region of very nonlinear mobility.

In addition, Persson [12] has recently used the molecular-dynamics (MD) technique to study a two-dimensional (2D) system of interacting atoms subjected to a 2D external periodic potential; this model may be considered as a generalized FK model. For the *underdamped* case $\eta \ll \omega_0$, he observed a dynamical transition: with increasing of the force F, the system presents a discontinuous transition from the low-mobility state B_0 to the high-mobility state B_f, and for decreasing force, the system exhibits a hysteresis. Because the value B_f corresponds to the maximum mobility of an isolated atom in a uniform space, the simulation results indicate that in the high-mobility state the system does not feel the external potential at all. Using the well known Aubry phase transition from the pinned state to the sliding state in the FK model in the case of incommensurate atomic concentrations [13], Persson supposed that the high-mobility state in his simulation corresponds to the incommensurate sliding state of the 2D system.

On the other hand, the Brownian motion of *noninteracting* atoms placed on a one-dimensional periodic potential and driven by the dc force F had been studied in a number of works [14–18]. It was shown that the crossover from the low-F mobility B_0 to the high-F mobility B_f depends on the friction coefficient η and the system temperature T. Indeed, when an atom is driven by the force F from one top of the total potential $V_{\mathrm{tot}}(x)$ to the next top in the absence of thermal fluctuations ($T=0$), it gains the energy $\varepsilon_+ = F a_s$ over one period, but at the same time it loses the energy $\varepsilon_- \sim \eta m \langle \dot{x} \rangle a_s$ because of damping. If $\varepsilon_+ > \varepsilon_-$, the atom will come finally to the ''running'' stationary state; in the opposite case $\varepsilon_+ < \varepsilon_-$, the final state will be ''locked.'' It is clear that the atomic motion is always running for the forces $F>F_\tau$, when $V_{\mathrm{tot}}(x)$ has no minima. In addition, there exists a second critical value F_η ($F_\eta \simeq 4\eta\sqrt{m\varepsilon_s}/\pi$) such that for $F<F_\eta$ the stationary state is always locked. The intermediate region $F_\eta<F<F_r$ is bistable: the motion is either running or locked depending on the initial velocity of the atom [19,14]. Thus, at $T=0$, the underdamped system of noninteracting atoms exhibits a dynamical first-order phase transition: when the external force increases, the system undergoes the locked-to-running transition at $F=F_r$ while, when the force is decreased, the reverse running-to-locked transition takes place at $F=F_\eta$. However, at any $T\neq 0$, the phase transition disappears because thermal fluctuations cause transitions of the system from the running to the locked state and back [20–22]. For a low fluctuation force and a temperature $T\simeq 0$, the bistable region is split into the running and locked subregions by a curve $F_c(\eta)$ [23]. When $F<F_c$, the system is mainly in the locked state where $B(F)\approx B_0$, while for $F>F_c$ the system is mainly in the running state and $B(F)\approx B_f$. Thus, when the force F increases crossing the value F_c, the mobility $B(F)$ changes sharply from B_0 to B_f. When the temperature of the system T is increased, this transition is smeared out.

Using these results, it is reasonable to suppose that the high-mobility state observed by Persson, corresponds not to the sliding state of the incommensurate FK model as it was proposed [12], but to the running state of atoms in the inclined substrate potential. However, the transition in the system of noninteracting atoms is not a phase transition but a smooth transition for any $T\neq 0$, while the transition observed by Persson is a first-order phase transition with hysteresis.

The aim of the present work is to study this transition in greater detail. We consider the generalized FK model, which describes the 2D system of interacting atoms subjected to the 3D external potential periodic in two dimensions and parabolic in the third dimension. The model may be used to describe a submonolayer film of atoms adsorbed on a crystal surface, so that the external potential corresponds to the substrate potential periodic in the directions parallel to the surface and parabolic in the direction orthogonal to it. The most interesting application of the model is connected with tribology problems [24] (e.g., the understanding of friction and lubrication between two flat macroscopic surfaces) as had been discussed in detail by Persson [12]. However, let us emphasize here that in the usual solid friction at a macroscopic scale, it is valid to use the zero-temperature approximation, since the heights of the energy barrier to be overcome are much greater than the thermal energy. Studies of usual solid friction in the presence of amplitude-controlled noise would deserve experimental investigation [25]. The behavior of the hysteresis should be qualitatively in agreement with results presented here in the context of microscopic friction where the effect of the temperature is very important.

Our results show that, contrary to the case of a single atom, in the system of interacting atoms the transition from the locked to the running regime becomes abrupt even at nonzero temperature, i.e., corresponds to a dynamical first-order phase transition. In addition, we found that there are intermediate states between the locked and running regimes. Using a phenomenological approach that treats a system of strongly interacting atoms as a system of weakly interacting quasiparticles (kinks), we estimate the thresholds for different concentrations and then we compare the simulation and estimation results. The results show also that at low T for the $\theta\neq 1$ case the nonlinear mobility $B(F)$ exhibits a hierarchy of steps.

We have organized this paper in the following way. The model, the choice of its parameters, and the numerical

method are described in Sec. II Sections III and IV form the heart of the paper. Simulation results are presented in Sec. III, while Sec. IV is devoted to the phenomenological approach of the problem. Finally, Sec. V discusses the results and conclusions.

II. THE MODEL

The displacement of an atom is characterized by three variables: x and y describe its motion parallel to the surface, while z describes its deviation orthogonal to the substrate. For the substrate potential, we take the function

$$V_{\rm sub}(x,y,z)=V_{\rm pr}(x;a_{sx},\varepsilon_{sx},s_x)+V_{\rm pr}(y;a_{sy},\varepsilon_{sy},s_y)+V_z(z), \tag{1}$$

where we use the deformable potential proposed by Peyrard and Remoissenet [26],

$$V_{\rm pr}(x;a,\varepsilon,s)=\frac{1}{2}\,\varepsilon\,\frac{(1+s)^2[1-\cos(2\pi x/a)]}{1+s^2-2s\,\cos(2\pi x/a)}, \tag{2}$$

which can be tuned to describe a real substrate potential rather accurately. Thus, $\varepsilon_{sx(y)}$ corresponds to the activation energy for diffusion of an isolated adatom on a substrate with the rectangular symmetry along the x or y direction, $a_{sx(y)}$ corresponds to the lattice constants, and the parameters $s_{x(y)}$ ($|s|<1$) describe the shape of the substrate potential. Namely, the frequency ω_x of a single-atom vibration along the x direction is connected to the shape parameter s_x by the relationship $\omega_x=\omega_0(1+s_x)/(1-s_x)$, where $\omega_0\equiv(\varepsilon_{sx}/2m)^{1/2}(2\pi/a_{sx})$.

The potential perpendicular to the surface is modeled by the parabolic function

$$V_z(z)=\tfrac{1}{2}m\omega_z^2z^2, \tag{3}$$

where ω_z is the frequency of normal vibration of an isolated adatom.

For the interaction between the atoms we take the exponential repulsion

$$V_{\rm int}(r)=V_0\exp(-\beta_0 r), \tag{4}$$

where V_0 is the amplitude and β_0^{-1} determines the typical range of the interaction. The potential $V_{\rm int}(r)$ corresponds to the usual repulsive branch of interatomic potentials that come into play when one attempts to pack atoms at an average distance smaller than their equilibrium distance. In numerical simulation we can include only the interaction of a given adatom with a finite number of neighbors. Therefore, we have to introduce a cutoff distance r^* and account only for the interaction between the atoms separated by distances lower than r^*, as is usual in MD simulations. To reduce errors caused by this procedure, we use instead of the interaction (4) the potential

$$\widetilde{V}_{\rm int}(r)=V_{\rm int}(r)-V_{\rm int}(r^*)-V'_{\rm int}(r^*)(r-r^*), \tag{5}$$

so that the potential and force vanish at the cutoff distance $\widetilde{V}_{\rm int}(r^*)=\widetilde{V}'_{\rm int}(r^*)=0$ (tilde will be omitted in what follows). In addition, because we are using the repulsive interatomic interaction, we have to impose periodic boundary conditions in the x and y directions in order to fix the atomic concentration. Therefore, we will place N atoms in the fixed area $L_x\times L_y$, where $L_x=M_xa_{sx}$ and $L_y=M_ya_{sy}$, so that the dimensionless atomic concentration (the so-called coverage in surface physics) is equal to $\theta=N/M$ ($M=M_xM_y$).

To model the energy exchange with a thermal bath, we use the Langevin equations for atomic coordinates x_i

$$m\ddot{x}_i+m\eta\dot{x}_i+\frac{d}{dx_i}\left[V_{\rm sub}(x_i,y_i,z_i)+\sum_{j(j\neq i)}V_{\rm int}(|\vec{r}_i-\vec{r}_j|)\right]=F^{(x)}+\delta F_i^{(x)}(t), \tag{6}$$

and similar equations for y and z. Here η corresponds to the rate of the energy exchange with the substrate, $\vec{F}=\{F,0,0\}$ to the dc driving force, and δF is the Gaussian random force with correlation function

$$\langle\delta F_i^{(\alpha)}(t)\,\delta F_j^{(\beta)}(t')\rangle=2\eta mk_BT\delta_{\alpha\beta}\delta_{ij}\delta(t-t'). \tag{7}$$

In the simulation we use a dimensional system of units, measuring distance in Angstroms, energy and temperature in electron volts. The mass of adatoms is chosen as unity $m=1$, which defines the time unit. In the result, the velocities are measured in units of $v_0=(1\ \text{eV}/m)^{1/2}$ and the force in units of $F_0=1$ eV/Å; we introduce also the characteristic time interval $t_0=2\pi/\omega_x$. In the remainder of the paper, the units of other dimensional physical quantities will be omitted, but they are expressed in terms of the above units.

In order to be closer to real physical systems, let us take the adsystem Na-W(112) as an example to define the model parameters. Namely, in the simulation, we put $a_{sx}=2.74$ Å and $a_{sy}=4.47$ Å, which are the distances between the neighboring wells along and across the furrows on the W(112) surface, respectively, and $\varepsilon_{sx}=0.46$ eV and $\varepsilon_{sy}=0.76$ eV for the corresponding barriers (these values were taken from [27]). To model the shape of the substrate potential, we have to know the parameters s_x and s_y. They lie usually within the interval [0.2, 0.4] [28]. For the sake of concreteness we took $s_x=0.2$ and $s_y=0.4$, which leads to the following frequencies of adatom vibrations: $\omega_x=1.65$ and $\omega_y=2.02$, respectively. For the vibration frequency normal to the surface, we took $\omega_z=\frac{1}{2}(\omega_x+\omega_y)=1.84$. Although these frequencies are taken rather arbitrarily, they are typical for metal atoms adsorbed on metal substrates [29,30]. For the interatomic potential (4), we took the parameters $V_0=10$ eV and $\beta_0=0.85$ Å^{-1}. This choice results in reasonable values for the adsystem [31], since the interaction energies between two adatoms, occupying the nearest wells along the furrow and across, are equal to $V_{\rm int}(a_{sx})\approx0.97$ eV and $V_{\rm int}(a_{sy})\approx0.22$ eV, respectively. Finally, we have to define the rate of energy exchange between the adatoms and substrate. We took $\eta=0.1\omega_x=0.165$ which again is a typical value [30]. Note, that our choice of the parameters does not claim to be a detailed quantitative interpretation of the Na-W(112) adsystem because the model is still oversimplified for real adsystems. However, we do believe in a qualitative description of the effect under investigation and claim that typical adsystems should exhibit similar behaviors. Finally, for a numerical solution to the Langevin equations (6), we use the stan-

dard fourth-order Runge-Kutta method with the time step $\Delta t = t_0/20 = 0.19$, and the cutoff radius is taken as $r^* = 2a_{sy} = 8.94$ Å.

III. SIMULATION RESULTS

A. Numerical procedure

In the simulation, we first look for the minimum-energy configuration of the system. Thus, we start with an appropriate initial configuration and allow the atoms to relax to the minimum of the total potential energy, keeping $T=0$ and $F=0$ (this procedure was described in detail in a previous work [32]). Then we increase the system temperature up to a given temperature T by small steps $\Delta T = T/50$ during the time $t_{\rm therm} = 100t_0$. At that point, we start to increase the dc force F by small steps $\Delta F = 0.01$ up to a value $F_{\rm max}$. At each step we wait the time $t_{\rm wait} = 100t_0$ in order to allow the system to reach a stationary state. Then, for the discrete times $t_i = it_0$, we measure the system characteristics such as the average velocity of the atoms $\langle v_x \rangle$ or the effective system temperature T_e defined by the equation

$$3\tfrac{1}{2}k_B T_c = \tfrac{1}{2}m \sum_{\alpha=x,y,z} \langle (v_\alpha - \langle v_\alpha \rangle)^2 \rangle. \tag{8}$$

The measures are carried out during the time $t_{\rm run} = 100t_0$, so that we get 100 points to compute averaged values for every value of F. In addition, at some steps we saved the coordinates and velocities of all atoms.

The external force is increased up to the value $F_{\rm max}$, and then decreased to zero with the same steps. In the simulation we mainly studied the system behavior for two substrate temperatures: zero temperature [in fact we used a very low but nonzero temperature $T=5.8$ K ($k_B T = 0.0005$ eV) for technical reasons] and room temperature $T=290$ K ($k_B T = 0.025$ eV). However, we also present results corresponding to different temperatures.

To simplify the study of the problem, we first begin from a simpler quasi-one-dimensional case, putting $M_y = 1$ so that all chains are moving in the same way (but the interaction between the atoms still has the 2D character). In the second part, we consider the full 3D case.

In the present work we restrict ourselves to concentrations within the interval $0.5 < \theta < 1$. The results for the trivial commensurate concentrations $\theta = 0.5$ and $\theta = 1$ are not included in the paper (although we made several runs for these cases too), because in these cases the $B(F)$ dependences exhibit only one transition from the locked state to the running regime at a relatively high threshold. At that point we emphasize that the results strongly depend on the atomic concentration of the system because of the essential role of the geometrical kinks. These excitations can be defined for any commensurate atomic structure $\theta_0 = \sigma/q$, where σ and q are relative prime integers. As background structure, we will extensively discuss here the coverages $\theta_0 = \frac{1}{2}$, $\theta_0 = \frac{2}{3}$, and the golden mean because of the Aubry transition, but we also studied other concentrations to clarify our understanding.

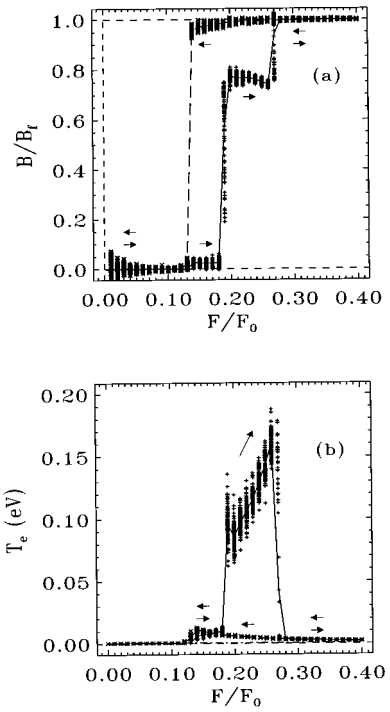

FIG. 1. *Hysteresis.* The mobility B is presented as a function of the external force F in (a), while (b) depicts the effective temperature T_e vs F (in fact we plot $k_B T_e$ measured in eV). The plus signs and the solid curve correspond to force increase, the cross signs and the dashed curve to force decrease. The arrows indicate the behavior of the mobility on increasing and decreasing the external force F. This picture corresponds to the quasi-one-dimensional system ($N=105$, $M_x=205$, and $M_y=1$), i.e., kinks on the background of the $\theta_0 = 1/2$ structure. The substrate temperature is $k_B T = 0.0005$ eV.

B. Quasi-one-dimensional FK model

1. Commensurate concentration

Let us first describe the results of simulations for the $\theta = 21/41$ case which corresponds to a system of kinks on the background of the $\theta_0 = 1/2$ structure. Namely, the $T=0$ ground state corresponds to a kink superstructure with average distance between the kinks equal to $41a_s$ (in simulation we took $N=105$ and $M_x=205$, thus having five kinks over the length under investigation). The $B(F)$ and $T_e(F)$ dependences for zero-substrate temperature are presented in Fig. 1 for F varying from zero to $F_{\rm max} = 0.40$. As seen from Fig. 1(a), with increasing force the system evolves from the locked state $B=0$ to the running state $B = B_f$, passing through two intermediate stages. The transition to the first intermediate state takes place at $F \approx 0.14$, the second transition occurs at $F \approx 0.20$, and the third transition to the running state is at $F \approx 0.28$. The behavior of the system exhibits a large hysteresis: when the force F decreases starting from $F_{\rm max}$, it remains in the running state down to $F \approx 0.14$ and then jumps directly to the locked state. At the same time, the effective temperature T_e [see Fig. 1(b)] increases at the intermediate states, while in the locked and running states it is close to zero.

All the transitions are discontinuous (at least with our resolution $\Delta F = 0.01$). In Fig. 2, we plot a stroboscopic map (an analog of the Poincaré section which is widely used in stochastic dynamics). Namely, during the time $t_{\rm run}$ for each

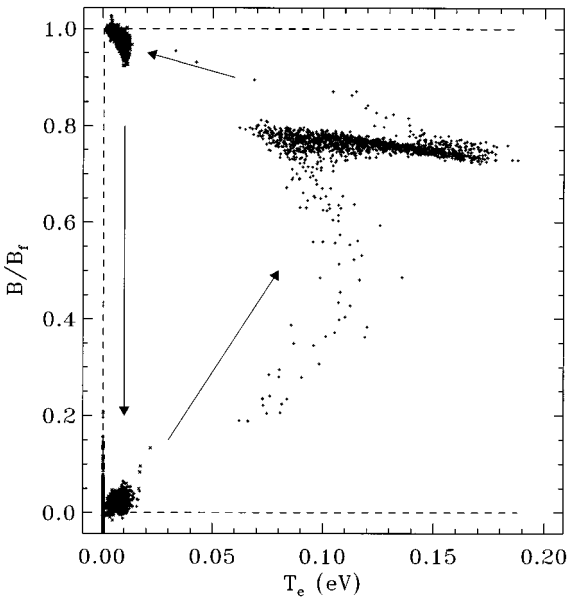

FIG. 2. Stroboscopic map in the (T_e, B) plane for the system evolution shown in Fig. 1.

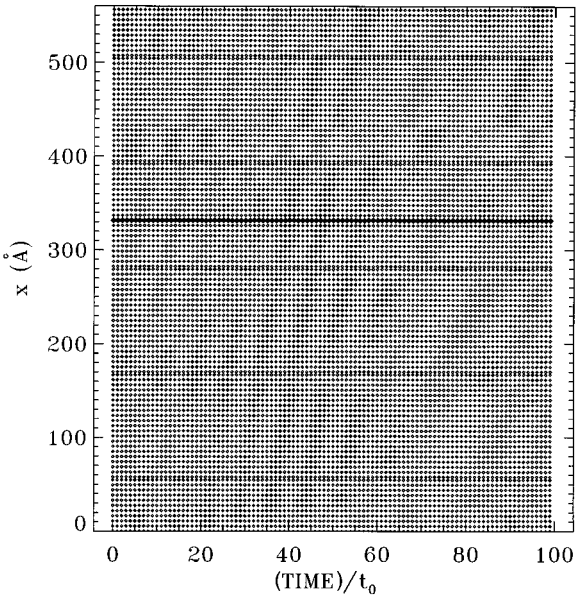

FIG. 3. *Static kinks.* Time dependence of the positions of all the atoms of the $\theta=21/41$ chain with periodic boundary condition for the $F=0.05$ step; curves are plotted for each t_0. Atom 62 is marked by filled diamonds to show clearly the trajectory of one atom. The darker regions correspond to increased atomic density, i.e., to kinks. The figure shows that neither the kinks, nor the individual atoms move for this low force.

step of force changing we saved the atomic velocities at the discrete time moments $t_i = it_0$, $i=1$ 100. To plot the sections, we chose the (T_e, B) plane, although another choice may be used as well. The resulting set of points is presented in Fig. 2, where we plotted all points in the same figure, so that it may be considered as the evolution of the steady-state system attractor with variation of the external force. The stroboscopic map shows few well-separated areas, one corresponding to the low-mobility regime with $B \approx B_0$ and $T_e \approx T$ ($B_0=0$ for the $T=0$ case), another to the running regime with $B \approx B_f$ and $T_e \approx T$, and also two intermediate areas.

Now let us describe the intermediate states in greater detail. Starting at a very low external force and switching on the force, the mobility remains zero. When we plot the atomic trajectories for $F=0.05$, we see in Fig. 3 that the atoms are in a completely frozen state: the black diamonds show explicitly that this atom and consequently all others are static. We can also distinguish the five topological defects, locked in their ground state, i.e., in the state where they are equidistant from one another. This picture verifies that the mobility is zero.

The first transition at $F=F_k \approx 0.14$ presents a hysteresis, too, as can be seen in Fig. 4(a), where we increase the external force up to the maximum value of 0.17 and then decrease the force. When we plot the atomic trajectories for the $F=0.17$ step in Fig. 4(b), we clearly see that the five topological defects are moving and one can even see a tendency of these kinks to come together (a similar effect for atoms will be described later in this section). However, the black diamonds showing the position of a single atom versus time emphasize that the atoms are moving much more slowly. Therefore, this first step corresponds to the transition between locked and running states *for the kinks* constructed on the background structure and the calculated mobility is nothing but the mobility of these kinks. This kink-running state survives up to $F \approx 0.19$ and is characterized by a mobility $B \approx 0.025 B_f$.

The second intermediate state exists within the interval $0.20 \lesssim F \lesssim 0.28$ and occupies the region $0.07 \lesssim k_B T_e \lesssim 0.18$ eV and $0.75 B_f \lesssim B \lesssim 0.85 B_f$ in the (T_e, B) plane. Simulation results show the following characteristic features of this state. First, it exhibits a well-defined hysteresis shown in Fig. 5, where we increase and then decrease the external force up to the maximum value of 0.20. Moreover, from the atomic trajectories, it is possible to see that this state corresponds to a regime of creation of kink-antikink pairs in addition to the first geometrical kinks. However, the different excitations are much more difficult to distinguish than in Fig. 4(b) and that is why we did not represent the picture here. Second, as can be seen from Fig. 6, the distribution of atomic velocities $P(v_x)$ shows two peaks, while the velocity distributions in the y and z directions (perpendicular to the chain) are Gaussian. It means that in the x direction some of the particles have a large velocity due to the external force in comparison with the values due to the temperature. Third, one can see that in the intermediate regime the mobility B is slightly decreasing when the force increases. This ''coexistence regime'' will be discussed in greater detail in Sec. IV D.

For a higher substrate temperature, the range of hysteresis decreases and at room temperature, we found no hysteresis for the $\theta=21/41$ case, as can be seen in Fig. 7. The mobility is still a strongly nonlinear function of the external force, but the transition is smooth. However, for a higher atomic concentration the hysteresis survives even at room temperature as, for example, in the $\theta=2/3+$kinks case where we took $N=105$ and $M_x=155$. The simulation results for this case are presented in Fig. 8. At zero temperature we may distinguish several steps on the $B(F)$ dependence (solid curve on the figure), which may be explained as those corresponding to transitions of superkinks and then trivial kinks to running

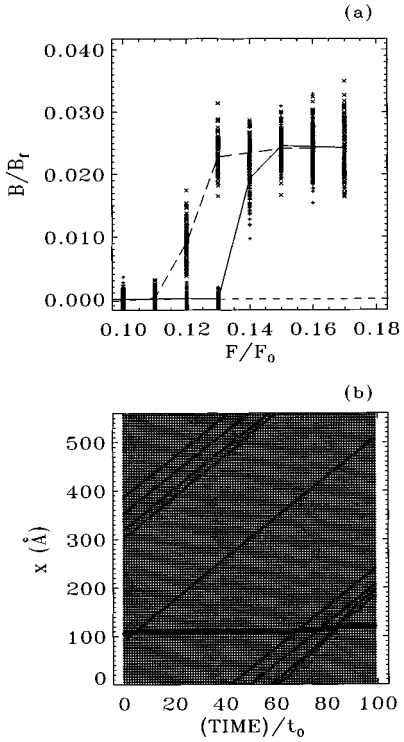

FIG. 4. *Running kinks.* The hysteresis of the mobility for $E_{max}=0.17$ in the $\theta=21/41$ chain at zero temperature is presented in (a), while time dependence of the positions of all the atoms of the $\theta=21/41$ chain with periodic boundary condition is plotted in (b); curves are plotted for each t_0 for the $F=0.17$ step. Atom 21 is marked by filled diamonds to show clearly the trajectory of one atom. The darker regions of increased atomic density (kinks) are now driven by the force. Individual atoms do not move except when a kink passes through their position as shown by the trajectory of the marked atom.

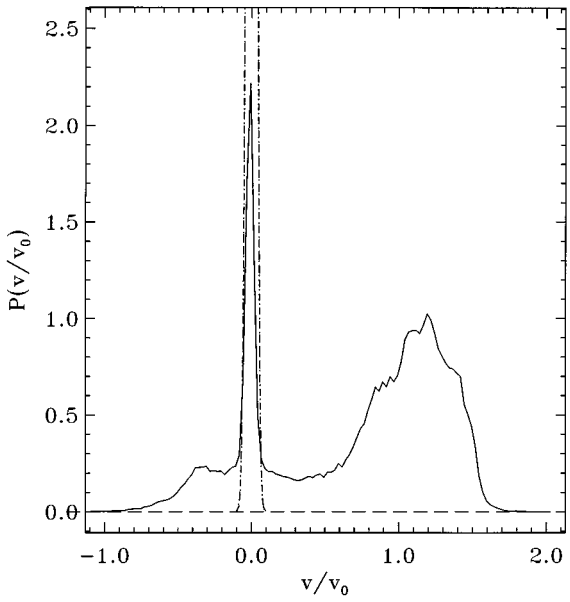

FIG. 6. Distribution of atomic velocities at $F=0.20$ for the $\theta=21/41$ case at zero substrate temperature. Full curve corresponds to $P(v_x)$, broken curve corresponds to $P(v_y)$, and dotted curve corresponds to $P(v_z)$.

states, as discussed in Sec. IV. At room temperature, the dotted curve shows that all abrupt transitions have disappeared owing to ''melting'' of the kink superstructures, and the $B(F)$ dependence becomes smooth. The effect of the temperature will also be discussed below.

2. Golden-mean concentration

The next simulation was made for the $\theta=34/47$ concentration (we took $N=170$ and $M_x=235$), which is close to the incommensurate concentration $\theta_{gm}=(3+\sqrt{5})/(5+\sqrt{5})$

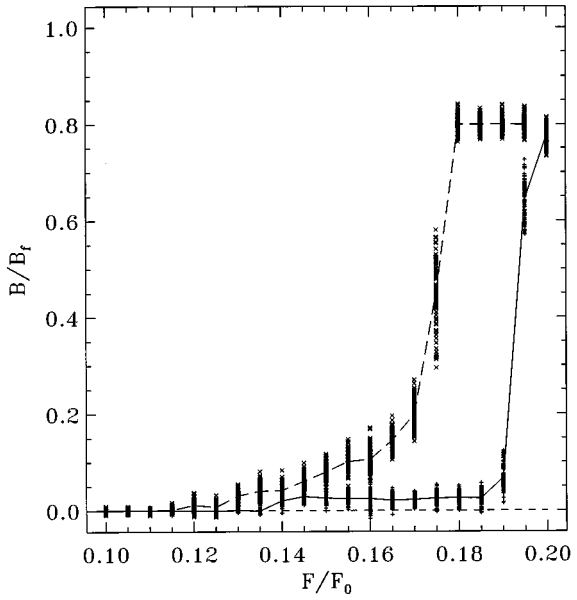

FIG. 5. *Creation of kink-antikink pairs.* The hysteresis of the mobility for $F_{max}=0.2$ in the $\theta=21/41$ chain at zero temperature.

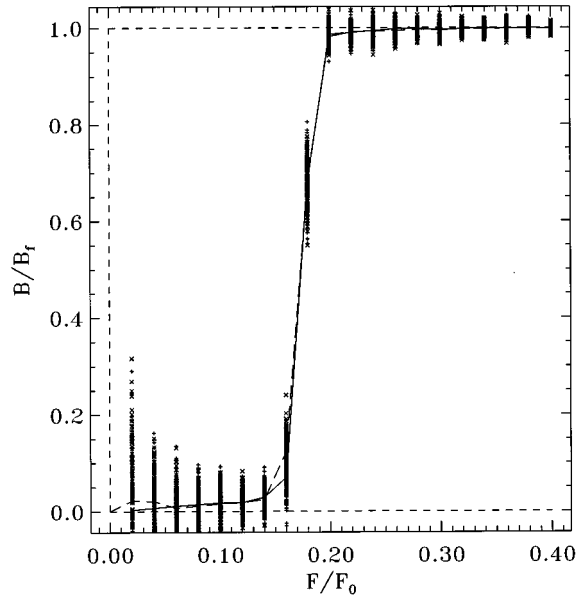

FIG. 7. Mobility B is presented as a function of the external force F. Same as Fig. 1(a), but for room temperature $k_BT=0.025$ eV.

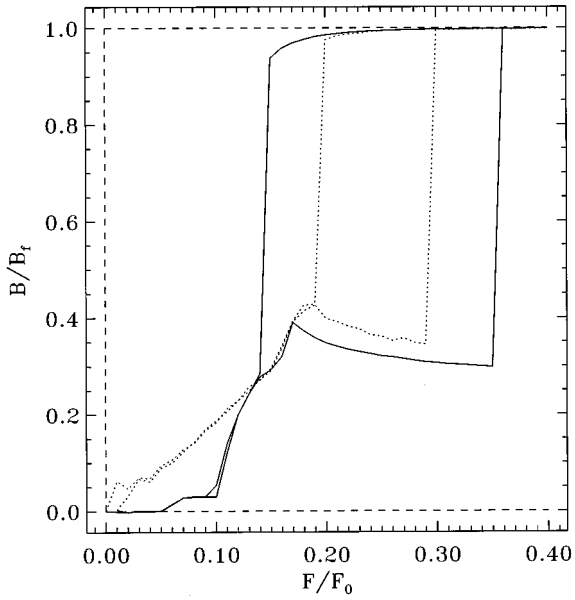

FIG. 8. Hysteresis of $B(F)$ for kinks on the $\theta_0=2/3$ background ($N=105$, $M_x=155$, and $M_y=1$). The solid curve corresponds to zero temperature and the dotted curve to room temperature.

≈ 0.724. As this noble irrational number is mathematically equivalent [33] to the golden mean, we also call it golden mean; if G is the golden mean, we have $\theta_{\rm gm}=(2+G)/(3+G)$. We recall that for an incommensurate concentration, Aubry showed that the $T=0$ ground state (GS) of the system may correspond to two different states depending on the magnitude of the average elastic constant $g_{\rm eff}$ [13]. For low $g_{\rm eff}$, $g_{\rm eff}<g_{\rm Aubry}$ (where $g_{\rm Aubry}\approx 1$ for $\theta=\theta_{\rm gm}$) the GS

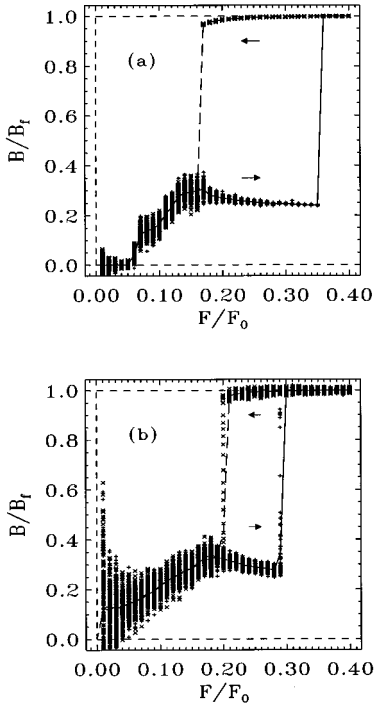

FIG. 9. Hysteresis of $B(F)$ for (a) zero temperature and (b) room temperature for kinks for the golden-mean $\theta=34/47$ case ($N=170$, $M_x=235$, and $M_y=1$).

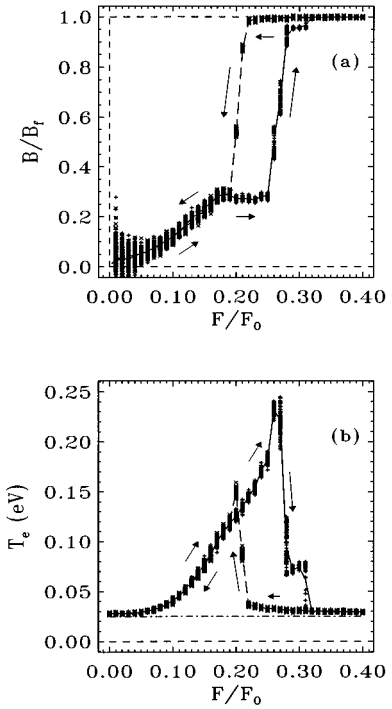

FIG. 10. The mobility B is plotted vs F in (a), while (b) presents the effective temperature T_e; both pictures correspond to the golden mean $\theta=34/47$ at room substrate temperature for the two-dimensional FK model ($N=1020$, $M_x=47$, and $M_y=30$).

is pinned, while for $g_{\rm eff}>g_{\rm Aubry}$, the GS is sliding and has no activation barrier for motion at any $F\neq 0$. For our choice of the model parameters we have $g_{\rm eff}\sim 0.24$, thus the system should be in the pinned state, but rather close to the Aubry transition point. Therefore, if the force is increased the system will reach the Aubry point owing to the lowering of the barriers of the inclined substrate potential. Indeed, simulation results presented in Fig. 9(a) show that the system exhibits nonzero mobility for a small force $F\approx 0.06$ in the case of zero-substrate temperature. However, we can see that just above the transition, the mobility is much smaller than the final mobility B_f, contrary to the infinite mobility expected for the frictionless $\eta=0$ case. When we further increase the external force F, the mobility B shows a slow increase, which should consist [34] of an infinite countable number of steps as for the Devil's staircase, but it is very difficult to study this behavior in detail. Then, at $F\approx 0.17$, the Devil's-staircase-like behavior is destroyed and, after the intermediate state corresponding to the kink-antikink nucleation regime, the mobility sharply increases to the maximum value $B\approx B_f$. Figure 9(b) shows that the hysteresis does exist at room temperature and is very similar to the $\theta=2/3$ case.

Thus, the main result of the quasi-one-dimensional simulations is that *for the chain of interacting atoms the hysteresis exists for any atomic concentration $\theta>0$ and survives for temperatures that are not too high*. Of course, these results deserve to be checked in the full two-dimensional FK model where M_y is not equal to one.

C. Two-dimensional FK model

1. Hysteresis of the mobility

At room temperature for the $\theta\approx\theta_{\rm gm}$ case, we took $N=1020$, $M_x=47$, and $M_y=30$, so that $\theta=34/47$ as in the

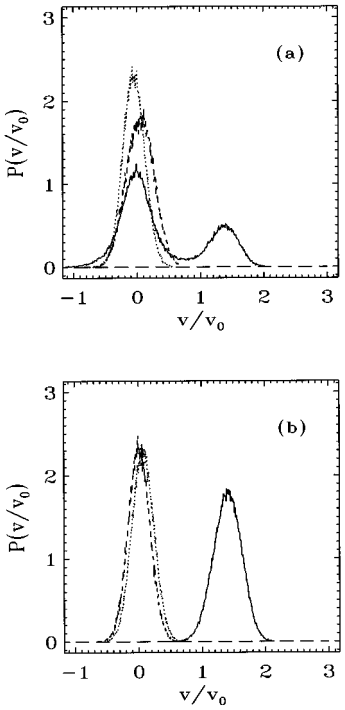

FIG. 11. Distribution of atomic velocities at the $F=0.24$ step for the two-dimensional $\theta=34/47$ model at room temperature. Full curve corresponds to $P(v_x)$, broken curve corresponds to $P(v_y)$, and dotted curve corresponds to $P(v_z)$. (a) corresponds to the state achieved during the force increase, and (b) to force decrease.

one-dimensional case described above. Figure 10 shows the $B(F)$ and $T_e(F)$ dependences for this case. We note that the 2D system displays a well-defined hysteresis too. The distribution of atomic velocities for the external force $F=0.24$ is presented in Fig. 11. On the one hand, in Fig. 11(a), for the state achieved with increasing force, there are two groups of atoms: one with velocities $v_x \sim v_y \sim v_z \sim v_{\text{thermal}}$ and another with velocities $v_y \sim v_z \sim v_{\text{thermal}}$ but $v_x \approx v_f \equiv F/m\eta$. On the other hand, in the state obtained for a decreasing force, all atoms are in the running state [see Fig. 11(b)], since there is only one bell curve for $P(v_x)$ centered around the value $v_f = F/m\eta$.

Surprisingly, we did not find essential differences between the behavior of the 1D and 2D systems. We recall that owing to interaction of kinks in the nearest neighboring (NN) channels, the NN kinks are arranged into domain walls (DW) or domain lines for the 2D system and this fact modifies the system-phase diagram as well as its dynamics [3]. For the repulsive interatomic interaction studied in the present work, kinks in the NN channels repel each other for the $\theta=1$ coverage, but for any $\theta<1$ the kinks are attractive and should be arranged in domain lines. However, for the short-range (exponential) interaction studied in our simulation, two kinks belonging to NN channels are attractive according to the law $V_{kk}(x) \propto |x|$, contrary to the usual widely studied law [3] $V_{kk}(x) \propto x^2$. That is why the DW stiffness in our model vanishes and the DW structure should be destroyed for any $T \neq 0$ or $F \neq 0$. Of course, in a more realistic 2D model with long-range interatomic forces such as elastic or dipole-dipole forces arising due to the substrate, the role of the DW structure might be more essential.

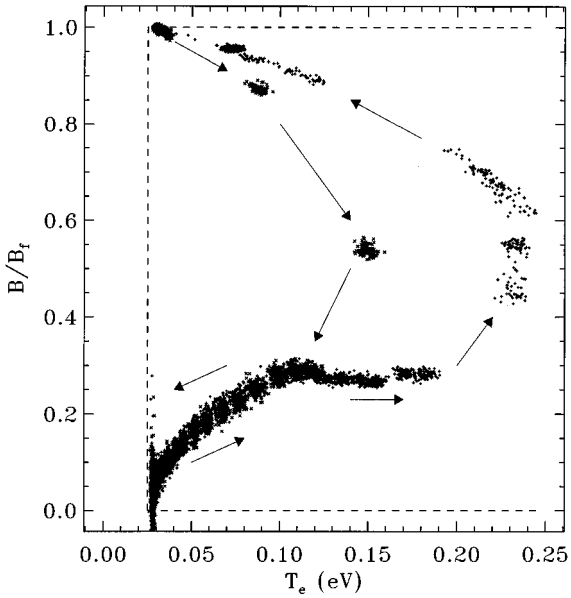

FIG. 12. Stroboscopic map in the (T_e, B) plane for the two-dimensional system $\theta=34/47$. The parameters are the same as in Fig. 11.

However, there are some differences with respect to the 1D case: comparison of Figs. 9(b) and 10(a) as well as the stroboscopic map of Fig. 12 shows that the transition in the 2D case is smoother than that in the 1D case described

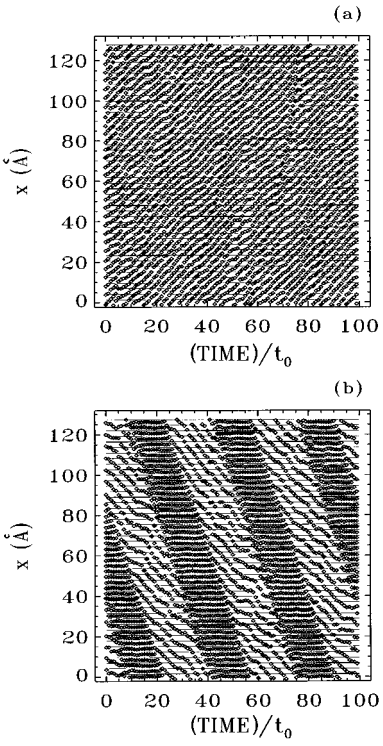

FIG. 13. Time dependence of the positions of all the atoms for the 2D system $\theta=34/47$ at $F=0.24$. (a) and (b) present two neighboring channels; curves are plotted for each t_0. The finite time interval between the snapshots results in a stroboscopic effect giving a wrong impression for atomic trajectory. In order to show one actual trajectory, one atom has been marked by black diamonds while others are indicated by unfilled diamonds.

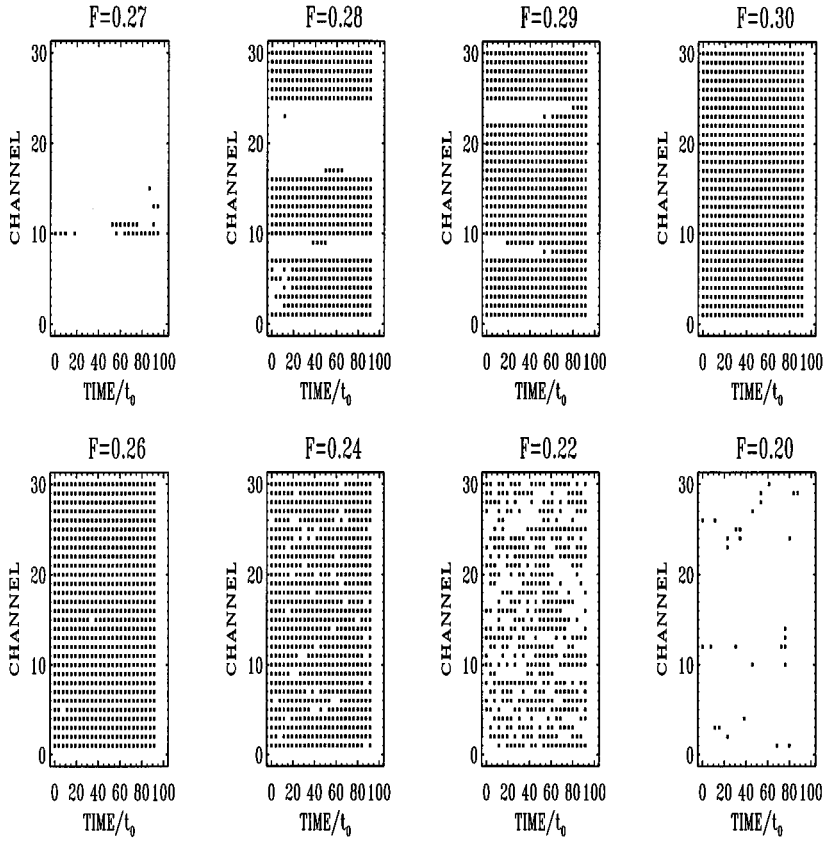

FIG. 14. *Growth of islands.* Moving channels (see text for definition) are represented with black points at different times. The pictures correspond to different external forces indicated by the title. The first four panels correspond to increasing force while the last four correspond to decreasing force.

above. When one looks at the atomic positions and velocities at a given time moment, one sees that in the 2D system the transition to the running state does not take place simultaneously in all channels, but due to thermal fluctuations it starts in a single channel (with a random number), while other channels remain in the coexistence regime where two groups of atoms exist. With further increase of the force, other channels are also transferred to the running state to: that is why, in the two-dimensional case, the region of the transition is smeared out. In subsection 2 we will study in greater detail the growth of these moving channels versus the external force.

2. Growth of moving islands

We studied the motion of atoms in different channels. Figure 13 shows, for example, the atomic trajectories for two neighboring lines in the x direction. The black diamonds emphasize the motion of one atom and clearly indicate two behaviors: in Fig. 13(a), the atom is always moving in the positive x direction, while in Fig. 13(b), the atom has an oscillatory behavior between the static and the running state; once the atom has reached a static group, it stays in this frozen state until its preceding atom has moved away, allowing the motion to begin again. It is interesting to note here the usual motion of cars in a traffic jam!

Now, let us look more carefully at the transversal growth of these moving regions. In the remainder of this paper, we will call *moving lines* the channels where all the atoms are moving, as is the case in Fig. 13(a). More precisely, we consider that a line is moving if, at a given time and for a given external force, all its atoms have a velocity greater than a threshold chosen between the two bells in the $P(v_x)$ plot [see Fig. 11(a)], namely, we have chosen $v_x>0.8$. Figure 14 presents the results for different forces; the ordinate is the index of the channel and the abscissa corresponds to several measurements. The black points correspond to moving channels, i.e., channels where all particle velocities are greater than the threshold.

First, we can see that the range of force is rather small between the first picture, where almost all lines are static ($F=0.27$), and the picture where the whole system is moving ($F=0.30$); therefore, to obtain quantitative results, we have to increase the force in very small increments. We can also see that, at the beginning, a few moving lines are created, not necessarily neighbors, and then for a slight force increase, these moving channels induce the motion of the neighboring channels, yielding an increase of the width of the moving island. The coalescence of the islands plays the final role. These illustrations also show an interesting difference between the dynamics during the increase of the force (first four panels) and, on the contrary, the dynamics during the decrease of the force (last four panels). We clearly see the horizontal lines in the first four panels, which means that if a channel is moving, it almost never stops. On the contrary, during decrease of the force, the dynamics is different, since one channel could move, be stopped just a small time later, and then move again; this generates a scattered picture.

To quantify these illustrations, we introduce the *width* of the moving islands as follows. Calling $w(i)$ the number of moving islands whose width is i channels, we define the quantity

$$\langle i\rangle=\frac{1}{M_y}\frac{\Sigma_i w(i) i}{\Sigma_i w(i)}. \tag{9}$$

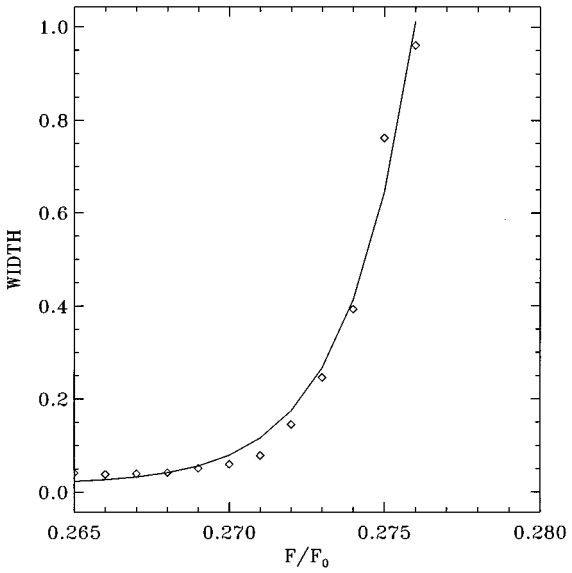

FIG. 15. For the case $\theta=21/31$, the diamonds depict the width of the moving island and the solid line corresponds to the approximate expression (see text).

The prefactor is used in order to have a definition independent of the transversal size of the lattice. In Fig. 15, the diamonds show the evolution of the width $\langle i \rangle$ versus the force in the case $\theta=21/31$, at room temperature. We used a lattice with 60 chains in the y direction in order to have good precision for the width because of the final exponential increase. We have fitted the width by the exponential $\exp[(F-F_0)/\Delta F]$. The solid curve in Fig. 15, corresponding to the values $F_0=0.276$ and $\Delta F=0.002$, shows that this expression is very accurate. We can also check that the value of F_0 corresponds to the transition to the running state, plotted in Fig. 9.

IV. DISCUSSION

A. Introduction and remarks

Now, let us show that most of the simulation results about the mobility of the FK system may be described in a similar way to the behavior of the system of noninteracting atoms if we consider kinks instead of atoms. The kink is a quasiparticle, characterized by its width d, an effective mass m_k and the rest energy ε_k. The kink can move along the chain but this motion is carried out in an effective Peierls-Nabarro (PN) potential with the amplitude $\varepsilon_{\rm pn}$. The kink parameters are determined by the dimensionless elastic constant $g_{\rm eff}$ defined as

$$g_{\rm eff}=\frac{a_{sx}^2}{2\pi^2\varepsilon_{sx}}\,V''_{\rm int}(a_A), \tag{10}$$

where $a_A=a_{sx}/\theta$ is the average interatomic distance along the chain. For our choice of the model parameters, we have $g_{\rm eff}\in[0.06,0.6]$ for the $\theta\in[0.5,1]$ coverages, so that the chain corresponds to the low-coupling limit and the kink parameters may be approximately calculated by the expressions presented in Ref. [7]. In particular, for kinks on the $\theta_0=\sigma/q$ background (σ and q are relative prime integers), the effective kink mass is equal to $m_k\approx m/q^2$. However, instead of using the approximate expressions for ε_k and $\varepsilon_{\rm pn}$, which are too crude in the case $g_{\rm eff}\sim1$, we have calculated these parameters numerically by the method described in detail in [35,36]. In particular, for kinks on the $\theta_0=1/2$ background we found $\varepsilon_{\rm pair}\equiv\varepsilon_k+\varepsilon_{\bar{k}}\approx0.759$ eV and $\varepsilon_{\rm pn}^{(k)}\approx0.0849$ eV. Now let us interpret the simulation results described in Sec. III, with the help of the quasiparticle-gas approach [37,7] valid at low temperatures $k_BT<\varepsilon_k$.

B. Geometrical kinks

For the $\theta=21/41$ case, the mass transport along the chain is carried out by ''trivial'' kinks constructed on the background of the $\theta_0=1/2$ structure as shown in Fig. 4(b); the position of the atom represented by black diamonds moves just for a few lattice sites while the five kinks almost completely cross the system during $100t_0$. As the averaged distance between the kinks is large (equal to $41a_{sx}$ in the ground state), the kink-kink interaction is small; the atomic flux is therefore restricted by the need for the kinks to overcome the PN barriers. When the driving force F is increased, the PN barriers are lowered [simultaneously with the original barriers of $V_{\rm tot}(x)$] in the direction of the force, resulting in the increase of the single kink mobility. So, at zero temperature the crossover from the locked $B_0=0$ state to the kink-running state is expected to take place at the force $F\sim F_k\approx C\pi\varepsilon_{\rm pn}/a_s$, where the factor C is approximately 1.15 for the chosen shape of the substrate potential (we assumed that the PN potential has the same shape as the original substrate potential). Substituting the value of $\varepsilon_{\rm pn}^{(k)}$ found numerically, we obtain $F_k\approx0.112$ which is close to the value $F_k\approx0.14$ found in the simulation. In addition, the kink-running state exactly coincides with the expected value of the mobility $B\approx\theta_kB_f$, where $\theta_k=1/41$ is the dimensionless kink concentration. Namely, we found $B/B_f=0.025$ as shown in Fig. 4(a). Moreover, this picture confirms that the mobility presents a hysteresis: the quasiparticle approach for the kinks is a very good description to explain this behavior.

For higher forces $F>F_k$, the residual-kink flux is saturated and an increase in mobility may be achieved owing to the creation of new kink-antikink pairs with their following motion in opposite directions. When force F increases, the energy threshold for the kk nucleation decreases from $\varepsilon_{\rm pair}$ to $\tilde{\varepsilon}_{\rm pair}=\varepsilon_{\rm pair}-Fx^*$, where x^* is the saddle point determined by the solution of the equation $v'_{k\bar{k}}(x)=F$ and $v_{k\bar{k}}(x)$ describes the energy of kink-antikink attraction (see details in [8]). The external force lowers the saddle-point energy, thus increasing the rate of kink-antikink pairs.

We know [38,35,7] that in the weak-coupling case the kink-antikink attraction at large distances behaves as $\tilde{v}_{k\bar{k}}(x)\propto\exp(-\gamma|x|)$, where $\gamma=\min(\xi/d,\beta_0)$, $\xi\approx-\sqrt{g_{\rm eff}}\ln g_{\rm eff}$, $d=a\sqrt{g_{\rm eff}}$ is the kink width, and $a=2a_{sx}$ is the period of the $\theta=1/2$ background structure. Because at short distances we have $\tilde{v}_{k\bar{k}}(0)=-\varepsilon_{\rm pair}$, we may use for the kink-antikink interaction the interpolating formula $\tilde{v}_{k\bar{k}}(x)\approx-\varepsilon_{\rm pair}/\cosh(\gamma x)$. In addition, in the discrete chain the kink motion is carried out in the PN potential

$$v_{\rm pn}(x) \approx \frac{\varepsilon_{\rm pn}^{(k)}}{2} \frac{(1+s^2)[1-\cos(2\pi x/a)]}{[1+s^2-2s\,\cos(2\pi x/a)]} \qquad (11)$$

so that the total potential for the $k\bar{k}$ pair nucleation may be written as $v_{k\bar{k}}(x) \approx \tilde{v}_{k\bar{k}}(x) + v_{\rm pn}(x)$. Using this expression, we obtain that the barrier for the $k\bar{k}$ nucleation is totally degraded at $F = F_{\rm pair} \approx 0.22$ which again is close to the simulation threshold $F_{\rm pair} \approx 0.20$.

C. Superkinks

Now let us consider within the quasiparticle-gas approach the more complicated case of the concentration $\theta = 21/31$. Numerical calculations for this coverage gave the values $\varepsilon_{\rm pair} \approx 0.170$ eV and $\varepsilon_{\rm pn}^{(k)} \approx 0.019$ eV. According to the phenomenological theory [7], the first step on the $B(F)$ curve should correspond to the transition of ''superkinks'', i.e., the kinks constructed on the background of the $\theta_0 = 2/3$ structure, to the running state; this step is therefore expected to take place at $F_{sk} \approx C\pi\varepsilon_{\rm pn}^{(k)}/a_{sx} = 0.025$, which may be compared with the simulation value 0.06. Then, the second increasing of $B(F)$ at $F = F_{sk\text{-pair}}$ will be associated with the creation of sk-$\bar{sk}$ pairs, but as we do not know the law for sk-$\bar{sk}$ interaction, unfortunately, we are unable to calculate it.

For higher external forces, $F > F_{sk\text{-pair}}$, the superkinks cannot be any longer considered as well-defined quasiparticles, because they are destroyed by the driving force. But now, we may consider the $\theta_0 = 2/3$ structure as a superstructure of the residual (''geometrical'') trivial kinks constructed on the background of the $\theta_0 = 1/2$ structure. Therefore, we may expect that the next increasing of $B(F)$ will take place at $F_{tk} \approx 0.14$, as we have found in the previous paragraph, and then at $F = F_{tk-\rm pair} \approx 0.22$, as it was for the $\theta = 1/2$ coverage. However, the mobility of the trivial kinks as well as the tk-$\bar{tk}$ nucleation rate is essentially suppressed owing to a huge concentration of residual kinks.

D. Coexistence regime

The transition of the system to the totally running state $B = B_f$ exhibits the existence of an intermediate state with a lower mobility B_m in the quite large interval of force $[F_{\rm pair}, F_r]$. This state, attributed in Sec. III B 1 to the regime of the creation of the kink-antikink pairs, will be called the coexistence regime because it corresponds to the coexistence of two groups of atoms: mobile and immobile. If this stage (as well as other intermediate stages) is not observed for the trivial coverages $\theta = 1/2$, $\theta = 1$, etc., it exists for all nontrivial coverages in the coverage interval studied [0.5, 1] and has some universal features. It is therefore interesting to dwell on its characteristics with the variation of coverage in greater detail. For simplicity, we will restrict our discussion to the quasi-one-dimensional FK model at low temperature $T = 0$, even if the discussion is also valid for the general 2D case and nonzero temperature.

Let us apply the kink-gas terminology to the description of this coexistence stage. First, we should note that at high enough values of force, corresponding to the state studied, we only have to consider the simplest kink excitations, namely, trivial kinks constructed on the background of the $\theta_0 = 1/2$ structure, for the entire coverage interval [0.5, 1], since other types of kinks (superkinks), which may exist in the coverage interval for lower forces, are much more subtle and are not well-defined quasiparticles for higher forces. For a given concentration θ, the coexistence stage is characterized by an approximately constant mobility B_m, lower than the maximum mobility B_f, when the applied force F is varied within a quite wide interval. A careful examination of the $B(F)$ dependences shows that the mobility B is even slightly decreasing with increasing force (see Figs. 1, 8, and 9). The maximum mobility at this stage occurs for lower forces, immediately after the kink-antikink nucleation threshold $F_{\rm pair}$. Then the kinks (the N_g geometrical kinks and the N_k force-excited kinks) start to bunch into compact groups and the decrease of the mobility can be understood in terms of the so-called *bunching* effect for kinks, introduced in the context of the Josephson-junction arrays where the kinks present a tendency to come closer together [39,40]. These compact groups of kinks are in fact dense immobile atomic islands with the coverage $\theta_i = 1$ (the subscript i and m mean immobile and mobile, respectively). With the gradual increase of the applied force (note, that according to the numerical procedure, the evolution time increases too), one can expect that the mobility will slightly decrease to some saturation value B_m due to the coalescence of these immobile islands of atoms. Indeed, as explained in the next paragraph, the first atom of an immobile group has a lower energy barrier to escape from this group, and therefore the number of completely locked atoms increases when immobile groups coalesce.

At the end of this coalescence process, the number of atoms in the immobile group is N_i. The rest of the system is mobile and consists of N_m mobile (or running) atoms with maximal possible velocity in the direction of force $v_f = B_f F$. It is remarkable, that the coverage θ_m in this mobile group of atoms was found to be constant, slightly lower than the kink-antikink background coverage $\theta_0 = 1/2$: the value is $\theta_m \approx 0.4$ within the studied interval [0.5, 1]. Let us emphasize that if the explanation is derived here in the one-dimensional case, the generic picture Fig. 13(b) corresponding to the two-dimensional case verifies that this value is also valid in the 2D case.

It is clear that N_i and N_m satisfy the relations

$$N_i + N_m = N, \quad M_i + M_m = M_x, \qquad (12)$$

where N is the total number of atoms in the system, $M_i = N_i/\theta_i$ ($M_m = N_m/\theta_m$) are the sizes of the parts of the system occupied by the immobile (mobile) subsystem, and M_x is the total system size.

Thus the system in the coexistence regime is split into two subsystems, namely, a dense immobile group with a coverage $\theta_i = 1$ and a mobile subsystem where the atoms are dynamically arranged in more-or-less regular structure with $\theta_m \approx 0.4$. Therefore, the total mobility of the system in the coexistence regime is $B_m = (N_m/N)B_f$ and has a simple dependence on coverage.

Let us show how the expression for the function $B_m(\theta)$ and the condition $\theta_m = \text{const}$ arise from the kink-gas approach. For the mobile subsystem of size M_m consisting of N_m atoms, the number of antikinks defined on the background of $\theta_0 = \sigma/q$ structures is $N_{\bar{k}} = \sigma M_m - q N_m$, i.e., for

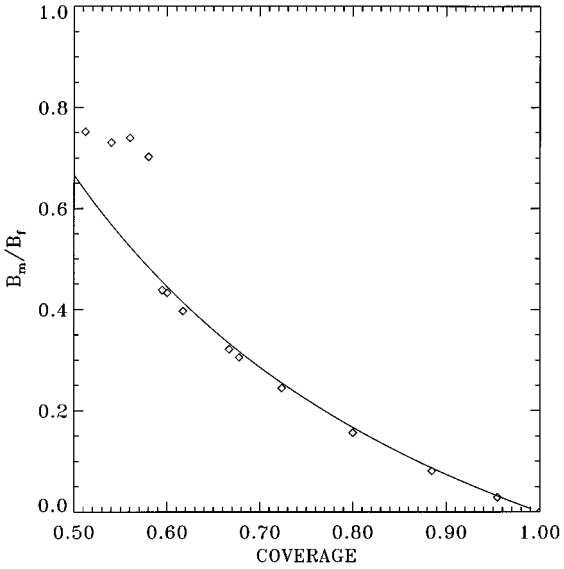

FIG. 16. Mobility B_m in the coexistence regime vs the coverage θ. The diamonds correspond to the simulation data and the solid curve to Eq. (14).

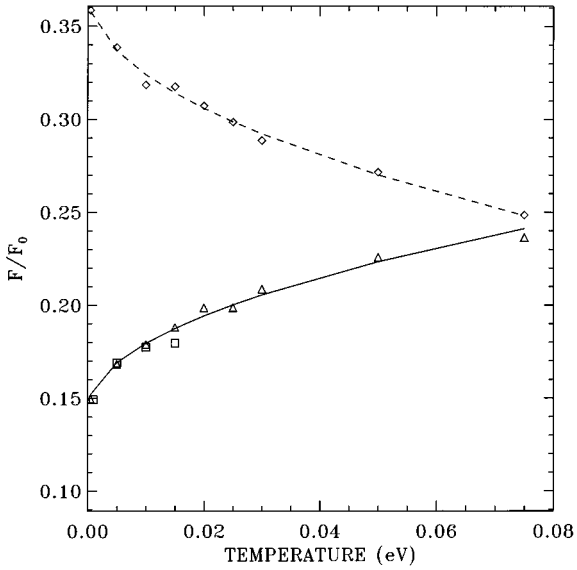

FIG. 17. Critical forces F_r^0 and F_b^0 at zero temperature vs coverage θ for $B=0.9B_f$.

our case, where $\theta_0=1/2$ and $N_{\bar{k}}=M_m-2N_m$. Combining this expression with Eq. (12) and using that for the dense immobile subsystem $M_i=N_i$ (since $\theta_i=1$), we obtain $N_m=M_x-N-N_{\bar{k}}$ and $M_m=2(M_x-N)-N_{\bar{k}}$. The last question is therefore to find the number of force-excited antikinks $N_{\bar{k}}$ depending on the total system size M_x and on the total number of atoms N.

For all coverages $1/2<\theta<1$ (i.e. $N>M_x/2$), there is always some excess of the atomic ''material'' needed to create new pairs of kinks and antikinks on the $\theta_0=1/2$ background structure. Therefore, in this coverage region, the main restriction on the number of the kink-antikink pairs $N_{\bar{k}}$, which can be excited in the system by some external factor (temperature, force), is the ''free room'' left in the system. Therefore, we can write $N_{\bar{k}}\simeq\alpha(M_x-N)$ where the constant α is lower than 1/2 and does not depend on both N and M_x. Physically, α corresponds to the saturation number for force-driven kink-antikink excitations at $F>F_{\rm pair}$ but it is, unfortunately, too difficult to estimate it reliably. Nevertheless, we obtain for the mobile subsystem $N_m=(M_x-N)(1-\alpha)$ and $M_m=(M_x-N)(2-\alpha)$; we are therefore able to derive the value of the coverage $\theta_m=N_m/M_m$ of the mobile subsystem

$$\theta_m=\frac{1-\alpha}{2-\alpha}=\text{const} \tag{13}$$

and the expression for the total mobility of the system $B_m=(N_m/N)B_f$ in the coexistence regime

$$B_m=B_f(1-\alpha)\,\frac{1-\theta}{\theta}=B_f\,\frac{\theta_m}{1-\theta_m}\,\frac{1-\theta}{\theta}. \tag{14}$$

Figure 16 shows the values of B_m obtained in simulation for various θ (symbols), and the approximate expression (14) for $\theta_m=0.4$ (solid curve). We see that this curve provides an excellent fit of the simulation data for almost all studied coverages [in the vicinity of $\theta=1/2$ coverage, the number of excited kink-antikink pairs deviates slightly from the simple expression $N_{\bar{k}}\simeq\alpha(M_x-N)$].

The coexistence of the mobile and immobile groups of atoms explains also the typical $T_e(F)$ dependence in this regime [see, e.g. Figs. 1(b) and 10(b)]. Indeed, the mean velocity in the immobile domain is of course zero while the mean-squared atomic velocity in the immobile domain is $v_i\approx\sqrt{k_BT/m}$. In the mobile domain, the mean velocity is $v_f\approx B_fF=F/m\eta$, while the mean-squared atomic velocity is $\sqrt{v_f^2+k_BT/m}$. Finally, substituting the mean velocity in the x direction $\langle v_x\rangle=(N_m/N)v_f$ into the expression of the effective system temperature defined by Eq. (8), it is easy to obtain that in the coexistence regime $T_e=T+[(N_m/N)(1-N_m/N)]mv_f^2/3k_B$. Thus, within the coexistence regime, the effective temperature T_e increases as F^2.

E. Critical forces

Now let us consider the coverage and temperature dependences of the forward critical force F_r for the transition from the coexistence regime to the totally running state, and the backward critical force F_b for the transition from the running state to the immobile state (or, for certain coverages, to the state with a nonzero mobility of the system, provided by kinks).

The dependences of F_r^0 and F_b^0 versus coverage θ at low temperature $T=0.0005$ are plotted in Fig. 17. It is seen, that at coverages $\theta=1/3$, $\theta=1/2$, $\theta=1$, etc., corresponding to the trivial ground states, the force F_r^0 is high and has values close to the value 0.6 for the case of noninteracting atoms. By contrast, the entire coverage interval [0.5,1] is characterized by reduced values of F_r^0, which are approximately two times lower than those for trivial coverages (apart from small variations probably arising from variations of the kink parameters with coverage). This difference is easy to understand if one takes into account the system's separation into dense immobile and more rarefied mobile groups of atoms

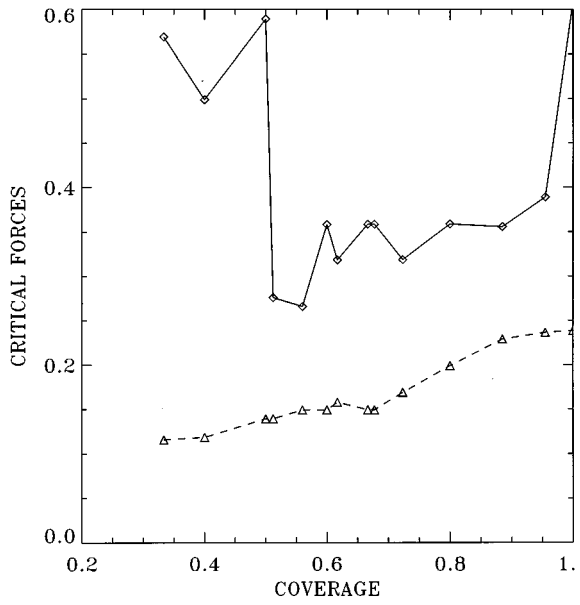

FIG. 18. *Width of hysteresis.* The diamonds (triangles) correspond to the position of the transition to the running (locked) state for different temperatures in the case $\theta=21/31$, while the squares corresponds to the transition to the locked state for $\theta=21/41$. The threshold was chosen to be $B=0.9B_f$. The solid and dashed curves correspond to the phenomenological approach discussed in the text.

during the coexistence regime. Indeed, because of the strong asymmetry of its environment (dense island behind it and rarefied island in front of it), the first atom of each immobile group has a much lower energy barrier to jump in the direction of the external force than in the case of a homogeneous film. Therefore, an inhomogeneous islandlike system in the coexistence regime $1/2<\theta<1$ is much easier to transfer to the running state than the homogeneous system at trivial coverages.

On the other hand, the force F_b^0 corresponding to the backward transition has a smoother dependence on the coverage (see Fig. 17). For low concentration, the transition to the locked state corresponds to the external force $F_b^0=4\eta\sqrt{m\varepsilon_s}/\pi$, as for noninteracting atoms. However, we see that this critical force increases with concentration: when the concentration is high, the particles are closer and the interaction potential becomes important, leading to an increase of the effective barrier between wells. It is interesting to note that for coverages less than $\theta\approx0.66$, the transition corresponds to a direct jump to the completely immobile state of the system, while for higher coverages the system jumps back to the state with a nonzero mobility; in the last case, a further decrease of the force yields the same decrease in the mobility as during the force-increasing process.

Let us show now that it is possible to derive the expression of the critical force F_b versus temperature. As discussed, at zero temperature the back transition approximately corresponds, for low concentration, to the external force $F_b^0=4\eta\sqrt{m\varepsilon_s}/\pi$. For nonvanishing temperatures, we can consider that the system goes to the locked state when the probability that the velocities will be lower than $F_b^0/m\eta$ is greater than a threshold P_0. Then, it is rather straightforward to derive that the critical force follows the law

$$F_b=F_b^0+\sqrt{2mk_BT\eta^2}\,\mathrm{erf}^{-1}(1-2P_c)$$
$$=F_b^0+\delta\sqrt{T}, \tag{15}$$

where erf^{-1} is the inverse of the error function. With $F_b^0=4\eta\sqrt{m\varepsilon_s}/\pi\simeq0.144$, the solid curve on Fig. 18 shows that this expression scales very accurately with the above expression if $\delta=0.35$.

The evolution of the forward transition versus temperature is much more complicated even if it is clear that because of the fluctuations due to the temperature, the particles will feel a smoother potential and a smaller barrier to overcome; therefore, the system will jump to the final running state for lower external forces. Numerical results plotted in Fig. 18 for the case $\theta=21/31$ scaled with the expression $F_r=F_r^0-\xi\sqrt{T}$, if we chose $F_r^0=0.37$ and $\xi=0.44$. While such a law is valid for other concentrations, the parameters significantly depend on the concentration, contrary to the law for F_b.

V. CONCLUSION

Let us now summarize the results, discuss their relations with other investigations of similar problems, and outline interesting topics for future studies. When an external force is increased, a system of interacting atoms exhibits a transition from the low-mobility regime with $B=B_0$ (the linear regime) to the high-mobility state with $B\approx B_f$. The latter regime corresponds to the running state of atoms in the inclined external potential, where the atoms gain more energy from the dc force than they can lose due to damping. The running regime may be achieved at high enough force for any atomic concentration θ; the high-B state does not correspond to the sliding state, contrary to the assumption of Persson [12], and therefore, it is not connected with incommensurability effects. This is confirmed by our results obtained at different coverages.

When $\theta=1/q$ so that the $T=0$ GS is trivial; there is no intermediate state; as in the case of noninteracting adatoms, the system goes directly from the locked to the running state. For a more complicated atomic structure $\theta=\sigma/q$ where $\sigma>1$, i.e., when the GS of the system may be considered as a hierarchy of subsequently ''melted'' superkink structures, the B_0-to-B_f transition passes through a series of intermediate states corresponding to the successive role of these superstructures. In particular, for an incommensurate GS, the system exhibits a devil's-staircase behavior [34].

The factor that restricts the system mobility is either the amplitude of the PN barriers, when the interparticle interaction is low, or the energy of kk pair creation, when the interaction is strong. The atoms in the intermediate states are split into two groups characterized by low and high velocities along the driving force. The high-velocity atoms are organized into compact groups, this fact is in accordance with the simulation results of [41] where the creation of new kk pairs was observed just behind the moving kink (domain line). Our simulations have also shown that the intermediate state is chaotic, although we did not study in detail the characteristics of the system attractor.

The transitions between different states are abrupt (first-order) even at nonzero temperature provided the corresponding superstructure is not melted at a given temperature. This

is the main difference between the system of interacting atoms and that consisting of noninteracting ones, where the transition is smooth for any $T \neq 0$. This fact may be explained in the following way: in a chain of interacting atoms, a single atom cannot jump alone from the locked state to the running state; the chain should jump as a whole between the different states. A more detailed investigation [42] of the simplified FK model showed that these transitions occurred through avalanches.

The present simulation has also shown that for any $\theta > 0$ and a temperature that is not too high, the $B(F)$ function exhibits hysteresis: the reverse B_f-to-B_0 transition takes place at a lower force $F = F_b$ than the direct transition. Again this effect may be explained as occurring owing to the collective character of motion in the system of interacting atoms. A single atom cannot jump from the running state to the locked state because it will be immediately pulled off by the neighboring running atoms. In connection with this question we have to mention the paper of Ariyasu and Bishop [43], where it was shown that during the force-decreasing process the SG system passes through a countable set of intermediate states corresponding to different concentrations of kink-antikink pairs.

Comparing the 1D and 2D systems, we did not find an essential difference in their behavior except that the 2D system exhibits smoother B_0-to-B_f transitions. This difference is connected with the fact that the transition in the 2D system does not take place simultaneously in the whole system, but starts in a single (random) channel and then is spread over other channels. Such an effect of creation of mobile atomic ''rivers'' when F is increased was studied earlier for the 2D system of atoms placed in the external potential of randomly distributed pinned impurities [44]. We have shown that the width of the rivers as a function of F scales with an exponential law.

The present work was initiated to an essential degree by Persson's papers [12], where similar questions were studied for 2D array of Xe atoms adsorbed on the Ag(100) surface. We emphasize, however, that Persson studied the *isotropic* 2D system, while we have investigated the *highly anisotropic* 2D array of atoms placed in 3D external potential, so the behavior of these two models might not be identical.

However, we made some simulations in the triangular case, which is one of the most isotropic lattices. Namely, we have taken the same energetic barriers in both transversal directions and have chosen the distance between channels equal to the distance between lattice sites in the x direction. The results showed that the hysteresis survived at nonzero temperatures even if the width of hysteresis decreased. However, the intermediate states have disappeared for the $\theta = 21/41$ coverage certainly because, in the triangular lattice, the interaction of neighboring kinks is different and gives rise to new dynamical features.

We confirmed one of Persson's results: the low-mobility–to–high-mobility transition is a first-order phase transition, i.e., is abrupt and exhibits the hysteresis even at nonzero temperature. In addition, we have shown that the high-B regime corresponds to the running state of the system and that the transition should pass through intermediate states. On the other hand, we do not confirm the relationship $F_{\text{back}} \approx 0.5 F_{\text{direct}}$ [12]. We also found that the increase of the effective temperature is due to the non-Gaussian velocity distribution in the intermediate states.

In this article, we have considered the nonlinear friction at an atomistic level. The role of the hysteresis is found to be crucial, as was found in mesoscopic friction [45,46]. Of course, since solid-state physicists and chemists have only recently begun to study the microscopic friction, new experiments and theoretical approaches are needed in order to complete our understanding, for example concerning the friction properties at the surfaces of two bodies. Work along this line is in progress.

ACKNOWLEDGMENT

O.M.B. is grateful to B. N. J. Persson for sending preprints of his works prior to publication.

[1] Ya. Frenkel and T. Kontorova, Phys. Z. Sowjetunion **13**, 1 (1938).
[2] H. R. Paneth, Phys. Rev. **80**, 708 (1950).
[3] I. F. Lyuksyutov, A. G. Naumovets, and V. L. Pokrovsky, *Two-Dimensional Crystals* (Naukova Dumka, Kiev, 1983).
[4] J. B. Boyce and B. A. Huberman, Phys. Rep. **51**, 189 (1979).
[5] St. Pnevmatikos, A. V. Savin, A. V. Zolotaryuk, Yu. S. Kivshar, and M. J. Velgakis, Phys. Rev. A **43**, 5518 (1991).
[6] O. M. Braun, T. Dauxois, M. V. Paliy, and M. Peyrard, Phys. Rev. B **54**, 321 (1996).
[7] O. M. Braun and Yu. S. Kivshar, Phys. Rev. B **50**, 13 388 (1994).
[8] M. Büttiker and R. Landauer, Phys. Rev. A **23**, 1397 (1981); M. Büttiker and T. Christen, Phys. Rev. Lett. **75**, 1895 (1995).
[9] F. Marchesoni, Phys. Rev. B **34**, 6536 (1986); P. Hänggi, F. Marchesoni, and P. Sodano, Phys. Rev. Lett. **60**, 2563 (1988); F. Marchesoni, Phys. Rev. Lett. **73**, 2394 (1994).
[10] S. E. Trullinger, M. D. Miller, R. A. Guyer, A. R. Bishop, F. Palmer, and J. A. Krumhansl, Phys. Rev. Lett. **40**, 206 (1978); **40**, 1603 (1978).
[11] R. A. Guyer and M. D. Miller, Phys. Rev. A **17**, 1774 (1978).
[12] B. N. J. Persson, Phys. Rev. Lett. **71**, 1212 (1993); Phys. Rev. B **48**, 18 140 (1993).
[13] S. Aubry, Physica D **7**, 240 (1983); M. Peyrard and S. Aubry, J. Phys. C **16**, 1593 (1983).
[14] T. Schneidner, E. P. Stoll, and R. Morf, Phys. Rev. B **18**, 1417 (1978).
[15] A. R. Bishop and S. E. Trullinger, Phys. Rev. B **17**, 2175 (1978).
[16] H. Risken and H. D. Vollmer, Z. Phys. B **33**, 297 (1979).
[17] H. D. Vollmer and H. Risken, Z. Phys. B **34**, 313 (1979).
[18] H. Risken, *The Fokker-Planck Equation* (Springer, Berlin, 1984).
[19] D. E. McCumber, J. Appl. Phys. **39**, 3113 (1968).
[20] E. Ben Jacob, D. J. Bergman, B. J. Matkowsky, and Z. Schuss, Phys. Rev. A **26**, 2805 (1982).

[21] M. Büttiker, E. P. Harris, and R. Landauer, Phys. Rev. B **28**, 1268 (1983).
[22] H. D. Vollmer and H. Risken, Z. Phys. B **52**, 259 (1983).
[23] H. D. Vollmer and H. Risken, Z. Phys. B **37**, 343 (1980).
[24] B. Brushan, J. N. Israelachvili, and U. Landman, Nature **374**, 607 (1995).
[25] J. Crassous (private communication).
[26] M. Peyrard and M. Remoissenet, Phys. Rev. B **26**, 2886 (1982).
[27] B. Bayat and H. W. Wassmuth, Surf. Sci. **133**, 1 (1983).
[28] O. M. Braun and E. A. Pashitsky, Poverkhn. (USSR) **7**, 49 (1984) [Phys. Chem. Mech. Surf. (UK) **3**, 1989 (1985)].
[29] A. Zangwill, *Physics at Surfaces* (Cambridge University Press, Cambridge, 1988).
[30] O. M. Braun, A. I. Volokitin, and V. P. Zhdanov, Usp. Fiz. Nauk. **158**, 421 (1989) [Sov. Phys. Usp. **32**, 605 (1989)].
[31] O. M. Braun and V. K. Medvedev, Usp. Fiz. Nauk **157**, 631 (1989) [Sov. Phys. Usp. **32**, 328 (1989)].
[32] O. M. Braun and M. Peyrard, Phys. Rev. B **51**, 17 158 (1995).
[33] G. H. Hardy and E. M. Wright, *Introduction to the Theory of Numbers* (Oxford University, Press, Oxford 1979).
[34] S. Aubry (unpublished).
[35] O. M. Braun, Yu. S. Kivshar, and I. I. Zelenskaya, Phys. Rev. B **41**, 7118 (1990).
[36] O. M. Braun, T. Dauxois, and M. Peyrard, Phys. Rev. B **54**, 313 (1996).
[37] J. F. Currie, J. A. Krumhansl, A. R. Bishop, and S. E. Trullinger, Phys. Rev. B **22**, 477 (1980).
[38] Y. Hsu, Phys. Rev. D **22**, 1394 (1980).
[39] A. V. Ustinov *et al.*, Europhys. Lett. **19**, 63 (1992).
[40] B. A. Malomed, Phys. Rev. B **47**, 1111 (1993).
[41] J. Pouget, S. Aubry, A. R. Bishop, and P. S. Lomdahl, Phys. Rev. B **39**, 9500 (1989).
[42] F.-J. Elmer, Phys. Rev. E **50**, 4470 (1994).
[43] J. C. Ariyasu and A. R. Bishop, Phys. Rev. B **35**, 3207 (1987).
[44] H. J. Jensen, in *Phase Transitions and Relaxation in Systems with Competing Energy Scales*, edited by T. Riste and D. Scherrington (Kluwer, Dordrecht, 1993), p. 129.
[45] C. Caroli and P. Nozieres, in *Physics of Sliding Friction*, edited by B. N. J. Persson and E. Tossati (Kluwer, Dordrecht, 1996).
[46] J. Crassous, E. Charlaix, S. Ciliberto, and C. Laroche (unpublished).